For time scales long compared to one orbital period, the trapped proton fluences are obtained from

$$T(h,i;E;\tau)=T_1(h,i;E)\times\tau \tag{3}$$

where T_1 is an annual trapped proton fluence and τ is the mission duration in units of years.

With Eqs. (2) and (3), the ratio R may be rewritten as

$$R(h,i;E;\tau,Q)=R_1(h,i;E)R_2(E;\tau,Q) \tag{4}$$

where $R_1=S_1S_2/T_1$ and $R_2=\tau^{-1}\times(S_3+S_4/S_2)$. The R_1 functions have the significance of being the solar-to-trapped proton fluence ratios for 1-year missions for which exactly one anomalously large event must be anticipated. R_1 functions are plotted in Figs. 1a-1d in terms of iso-ratio contours in h-i space for a series of energy thresholds. The R_2 functions are R_1 modifiers, adjusting the ratios to reflect the Q, τ dependent variation in mission duration and in the number of anomalously large events to be expected. Values of R_2 are inserted in matrix form into Figs. 1a-1d for mission duration between 2 months and 5 years and for risk factors between 0.01 and 0.1 (1 and 10%). Note that R_2 values are independent of energy for all Q, τ matrix elements except for the 5 and 10% risk factors of the 2-month missions, for which no anomalously large event is predicted. For all other elements, $S_3>0$ and S_4/S_2 becomes insignificant.

Discussion

The accuracy of the figures reflects the accuracy of the models used. As discussed in Ref. 4, the common geomagnetic cutoff assumption of the solar proton model used is reasonable for protons of less than 100 MeV, but becomes progressively less accurate as energies increase above 100 MeV. Thus, in Fig. 1d, the R_1 function may be underestimated by a factor of up to two. Likewise, there is a typical uncertainty by a factor of about two in the trapped proton model used.

Many features are immediately visible in the figures. First of all, the solar-to-trapped ratio is zero for orbits in the shaded areas where, by virtue of geomagnetic shielding, no solar particle reaches a spacecraft anywhere along its orbit. In the cross hatched region (high altitude, low inclination) the ratio is meaningless because neither solar nor trapped protons reach the spacecraft.

At a fixed altitude (below a few hundred km or so) the dominant fluence source shifts rapidly from trapped to solar protons as orbit inclination is increased through the 50° to 60° range. Thus, for low-altitude, polar-orbiting spacecraft, solar protons are very important relative to trapped protons. As the altitude of a polar orbit mission is increased, the solar-to-trapped ratio declines and then increases again. This is mainly due to the low latitude portion of the orbit moving out to, and then beyond, the regions of maximum trapped particle fluxes. The energy dependence of R_1, apparent from a sequential examination of Figs. 1a-1d, results from the variability of the trapped proton spectrum at differing spatial points and the dissimilarity of the trapped and solar spectra.

By examination of the inset matrices in Figs. 1a-1d, it is apparent that for a fixed risk factor, solar particles tend to become relatively less important than trapped particles as mission duration increases. At fixed mission duration, however, solar protons become relatively more important than trapped particles as the permissible risk factor is decreased. Note, however, that as long as at least one anomalously large event is anticipated, the variation in the solar-to-trapped ratio due to the mission duration and risk factor dependences is very small relative to the variation associated with the altitude and inclination dependences.

Conclusions

The purpose of the analysis has been to permit the space mission planner to readily determine whether he must consider solar and trapped proton fluences, or only one or the other, in his shielding requirements. The analysis is not intended to provide actual fluence values, which are available in the references cited.

The mission planner must specify orbit altitude and inclination (circular orbits only), mission duration, and the percent risk he is willing to take that the actually encountered solar proton fluence will exceed his design fluence. Then from the appropriate figure for the energy threshold of interest, he multiplies the appropriate factor from the inset matrix by the appropriate plotted R_1 value in order to determine the ratio of solar-to-trapped proton fluences he must allow for in his mission planning. Typically, interpolation will be required.

It is clear that for low-altitude polar and very high-altitude missions (any inclination), solar protons dominate trapped protons. Conversely, for low-inclination, low- and medium-altitude missions and for high-inclination, medium-altitude missions, trapped protons dominate the solar protons.

Due to the uncertainties in the models, we would recommend that if the value of the S/T ratio fell between 0.1 and 10, the mission planner ought to consider both trapped and solar proton fluences. Likewise, if the desired h, i point is in a region of rapidly changing S/T ratio, both trapped and solar fluxes should be considered.

References

[1] King, J.H., "Solar Proton Fluences for 1977-1983 Space Missions," *Journal of Spacecraft and Rockets,* Vol. 11, June 1974, pp. 401-408.

[2] Lavine, J. P. and Vette, J. I., "Models of the Trapped Radiation Environment, Vol. V: Inner Belt Protons," SP-3024, 1969, NASA.

[3] Lavine, J. P and Vette, J. I., "Models of the Trapped Radiation Environment, Vol. Vi: High Energy Protons," SP-3024, 1970, NASA.

[4] Stassinopoulos, E. G., and King, J. H., "Empirical Solar Proton Model for Orbiting Spacecraft Application," *IEEE Transactions on Aerospace and Electronic Systems,* Vol. AES-10, July 1974, pp. 442-450.

Errors in Aerodynamic Heat Transfer Measurements when Using Phase Change Coating Techniques

John A. Segletes*
Teledyne Isotopes, Timonium, Md.

Nomenclature

CF	=	correction factor
h	=	heat transfer coefficient
k	=	thermal conductivity
T	=	temperature
x	=	distance from surface
X, Y, τ	=	see Eq. 1
α	=	thermal diffusivity
θ	=	time

Received September 20, 1974; revision received Oct. 29, 1974. The work reported was supported under AEC Contract AT (49-15)-3069.

Index categories: Heat Conduction, Thermal Modeling and Experimental Thermal Simulation.

*Aerothermal Engineer, Safety and Reliability. Member AIAA.

Subscripts

m = phase change
o = initial
r = recovery
1-D = based on one-dimensional analysis
2-D = based on two-dimensional analysis

Introduction

A PHASE change coating technique has been used at the NASA Langley Research Center from 1958[1] until recently [2-4] to obtain quantitative aerodynamic heat transfer data. In its usual form, this technique employs a thin surface coating of material applied to a thermally thick model, i.e., a model having a wall thickness sufficiently large so that its back face will effectively not rise in temperature during the test. The coating undergoes a visible phase change at a known temperature. The precise time at which the change occurs is determined as a function of model surface location from an examination of motion pictures. The heat transfer coefficient distribution is then determined from one-dimensional exact solutions of a semi-infinite solid responding to a uniform temperature convective environment.

Implicit in the use of phase change coating techniques is the assumption that the heat transfer remains one-dimensional. In this study it is shown that a one-dimensional heat transfer assumption may lead to large errors in the measurement on local heat transfer coefficients. Specifically, the influence of two-dimensional heat transfer is examined in the vicinity of 90° and 120° corners. Correction factors to apply to one-dimensional results at the corners are determined.

One-Dimensional Solution

The solution of the one-dimensional transient heat transfer equation which satisfies the boundary conditions of a semi-inifinite solid exposed to a uniform temperature convective environment is given by the following:[5]

$$\tau = \text{erfc}\, X - e^{2XY+Y^2}\text{erfc}\,(X+Y) \tag{1}$$

where

$$\tau = (T_m - T_0)/T_r - T_0$$

$$X = (x)/[2(\alpha\theta)^{1/2}]$$

$$Y = (h/k)[(\alpha\theta)^{1/2}]$$

At the surface $X=0$. Therefore, Eq. (1) becomes the following at the surface:

$$\tau = 1 - e^{Y^2}\text{erfc}\ Y \tag{2}$$

Given the thermal properties of the model (k,α), the recovery temperature of the stream (T_r), the initial temperature of the model (T_0), the phase change temperature of the coating (T_m) and the test time required to change phase $(\theta=\theta_m)$, Eq. (2) may be solved for the heat transfer coefficient (h) existing at the surface.

Two-Dimensional Solutions

Two- and three-dimensional exact solutions corresponding to Eq. (1) do not exist. However, accurate solutions in regions of multi-dimensional heat flow may be obtained with the use of finite difference methods. In this study two-dimensional heat transfer in the vicinity of 90° and 120° corners is evaluated and compared with corresponding one-dimensional solutions.

Analytical models are shown in Fig. 1. The one-dimensional model was used to obtain reference solutions,

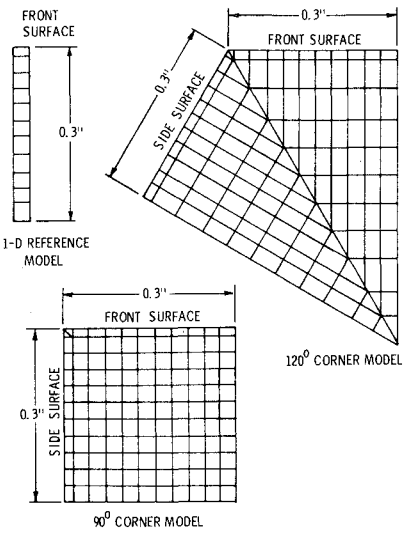

Fig. 1 Analytical models. Unit thickness—all models.

which, if accurate, will duplicate the solutions obtained by Eq. (1). Solutions were obtained using the Thermal Analyzer Program (TAP) for several values of heat transfer coefficient ratio $(h_{\text{side}}/h_{\text{front}})$. Here the subscript "front" refers to the two-dimensional model's heated surface which is under study. The subscript "side" refers to the other heated surface. The corner temperature was obtained by an extrapolation of surface temperatures along the surface with the higher h value.

To obtain accurate solutions over a wide range of Y it was found necessary to compute each case with three different values of k, then patch together those portions of each k solution which were determined to be accurate. This approach was necessary because it was found that a large k value resulted in accurate solutions for small Y values; however, the model did not remain thermally thick for large Y values. On the other hand, a small k value resulted in a thermally thick model for all Y's, but the solutions were inaccurate for small Y values. The latter inaccuracy is attributed to problem start-up which is discussed in Ref. 5.

Results

The procedure used for reducing the data was to plot corner temperature responses as shown in Fig. 2 for the 120° corner cases. Those responses to the left of the one-dimensional solution reach T_m sooner and hence have a higher apparent heat transfer coefficient than the one-dimensional solution. The one solution to the right reaches T_m later and hence has a

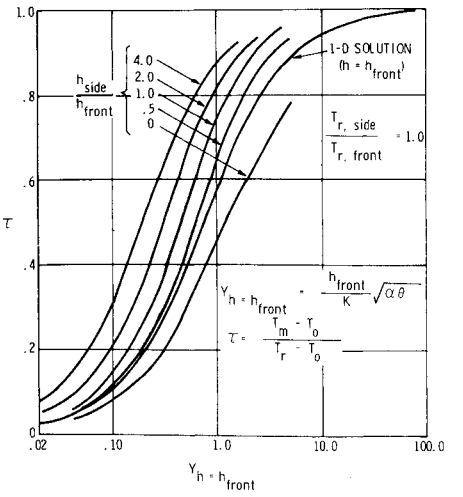

Fig. 2 Temperature responses at 120° corner.

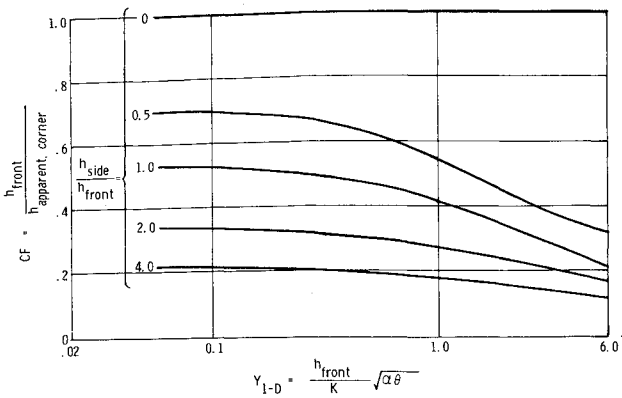

Fig. 3 Correction factor at corner-angle = 90°.

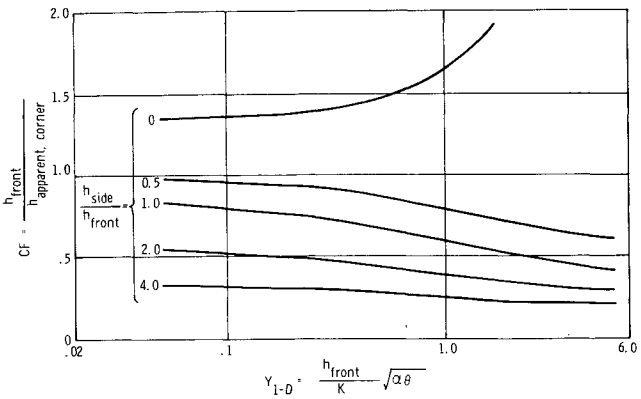

Fig. 4 Correction factor at corner-angle = 120°.

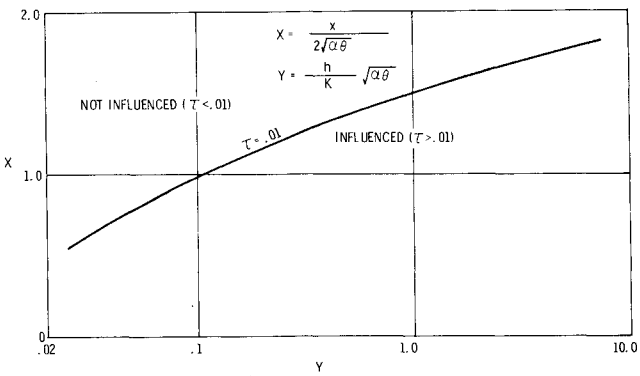

Fig. 5 Region of influence-one-dimensional solution (assumed to apply to 2-D solutions if x is taken as distance from corner.

lower apparent heat transfer coefficient than the one-dimensional solution.

The correction factor to apply to heat transfer coefficients obtained from one-dimensional solutions is given by the following relationship:

$$CF = \frac{h_{front}}{h_{apparent,\ corner}} = \left[\frac{Y_{2-D}}{Y_{1-D}}\right]_{\tau=\text{constant}} \quad (3)$$

Computed correction factors are presented in Figs. 3 and 4 as a function of Y_{1-D}.

It is apparent from the results that sizable errors may be realized by treating corners as one-dimensional problems. The error, of course, diminishes with distance from the corner. An estimate of the distance from the corner for which two-dimensional effects become negligible is obtained by solving Eq. (1) for $\tau = 0.01$. The results of this computation are shown in Fig. 5. An examination of actual results showed the rate of temperature propagation from the corner to be less than that given above.

This study assumed the recovery temperatures for the front and side surfaces were equal. In general, this is not the case. Higher recovery temperatures on the side surface than on the front will result in larger correction factors than those shown in Figs. 3 and 4. Conversely, lower side surface recovery temperatures will result in smaller correction factors.

References

[1] Jones, R. A. and Hunt, J. L., "Use of Fusible Temperature Indicators for Obtaining Quantitative Aerodynamic Heat-Transfer Data," TR R-230, Feb. 1966, NASA.

[2] Hunt, J. L., "Heat Transfer to Four Fineness-Ratio-1.6 Hexagonal Prisms with Various Corner Radi at Mach 6," TM X-2446, March 1972, NASA.

[3] Hunt, J. L., Pitts, J. L. and Richie, C. B., "Application of Phase-Change Technique to Thin Sections with Heating on Both Surfaces," TN D-7193, Aug. 1973, NASA.

[4] Creel, T. R., "Experimental Investigation at Mach 8 of the Effects of Projections and Cavities on Heat Transfer to a Model of the Viking Aeroshell," TM X-2941, April 1974, NASA.

[5] Carslae, H. S. and Jaeger, J. C., *Conduction of Heat in Solids*, 2nd ed., Oxford at the Clarendon Press, 1959, pp. 70-72, pp. 475-476.

Low Reynolds Number Effect on Hypersonic Lifting Body Turbulent Boundary Layers

J. C. Adams Jr.*
ARO, Inc., Arnold Air Force Station, Tenn.

Nomenclature

A_* = van Driest damping constant, 26.0
D = van Driest exponential damping function for the near wall region
k = inner law mixing-length constant, 0.435
£ = low Reynolds number mixing-length parameter
L = reference length
£ = mixing length
M_∞ = freestream Mach number
Pr_t = turbulent Prandtl number, 0.90
$Re_{e,\theta}$ = local Reynolds number based on inviscid edge conditions and boundary-layer momentum thickness
Re_∞/ft = freestream unit Reynolds number
St_∞ = local Stanton number based on freestream conditions

Received August 19, 1974; revision received October 29, 1974. The research reported herein was conducted by the Arnold Engineering Development Center (AEDC), Air Force Systems Command (AFSC), U.S. Air Force. Research results were obtained by personnel of ARO, Inc., contract operator of AEDC. Further reproduction is authorized to satisfy needs of the U.S. Government.

Index categories: Boundary Layers and Convective Heat Transfer—Turbulent; Supersonic and Hypersonic Flow.

*Senior Scientist and Supervisor, Project Support and Special Studies Section, Aerodynamics Projects Branch, von Karman Gas Dynamics Facility. Associate Fellow AIAA.